Estimation of Biomass Burned Areas Using Multiple-Satellite-Observed Active Fires

Xiaoyang Zhang, Shobha Kondragunta, and Brad Quayle

***Abstract*—Biomass burning releases a significant amount of trace gases and aerosols into the atmosphere and affects climate change, carbon cycle, and air quality. Accurate estimates of emissions depend strongly on the calculations of burned areas. Here, we present an algorithm that is used to derive burned areas by blending active fire observations from multiple satellites which are provided in the Hazard Mapping System (HMS). The HMS consolidates automated fire detections from Geostationary Operational Environmental Satellite (GOES) Imager, Advanced Very High Resolution Radiometer (AVHRR), and MODerate resolution Imaging Spectroradiometer (MODIS). Our goals are to derive burned areas in each GOES fire pixel across contiguous United States (CONUS) from 2004 to 2007 and to validate the estimates using Landsat Thematic Mapper/Enhanced Thematic Mapper plus (TM/ETM+) burn scars and National Fire Inventory data. The results show that annual fire events burn 0.4% (3.4×10^4 km^2) of total land across CONUS, which consists of 0.49% of total forests, 0.64% of savannas, 0.68% of shrublands, 0.40% of grasslands, and 0.30% of croplands. The large burned areas are dominantly distributed in the western CONUS, followed by the states in the southeast region and along the Mississippi Valley. Extensive validation shows that MODIS+AVHRR+GOES instruments greatly improve the determination of fire duration and fire detection rate compared to single instrument detections. The detection rate of small fire events (< 10 km^2) from multiple instruments is 24% and 36% higher than that from MODIS and GOES, respectively. The error in the burned-area estimate is less than 30% in individual ecosystems, and it decreases exponentially with the increase of burn scar size. Overall, the accuracy of total burned area across CONUS is 98.9% when compared to TM/ETM+-based burn scars and 83% when compared to national inventory data.**

***Index Terms*—Active fires, burned areas, fire duration, fire size, multiple satellites, validation.**

I. Introduction

VEGETATION burned area is a key input to estimate greenhouse gases and aerosols released from fires into the atmosphere, which have short- and long-term impacts on the global carbon cycle and air quality [1]. Furthermore, the vegetation burned area can cause the conversion and the alteration of various ecosystems [2] and can seriously affect hydrologic and ecological environments, such as the increase of soil erosion [3]. However, burned areas are traditionally not well recorded in large regions because field measurements are time consuming, expensive, and difficult [4]. Satellite data overcome some of the traditional limitations by providing observations of instantaneous fire hotspots and postfire burn scars on regional and global scales.

Biomass burned area is well quantified from remotely sensed burn scars and active fires, although the process is complex and challenging. Burn scar is the area affected by a fire event, which can be obtained by comparing the variations in spectral reflectance and vegetation index between pre- and postfires [5], [6]. At regional and global scales, the areas of burn scars in postfires have been estimated from moderate-resolution data ($\sim$1 km) by analyzing subpixel Advanced Very High Resolution Radiometer (AVHRR) properties [7], by comparing the variations in daily or ten-day AVHRR Normalized Difference Vegetation Index data [8], [9], and by investigating daily or monthly Systeme Pour l'Observation de la Terre (SPOT) VEGETATION (VGT) [10], [11]. Similarly, burn scars have been routinely retrieved globally from MODerate resolution Imaging Spectroradiometer (MODIS) data since 2001 [12], [13]. These moderate-resolution data can reasonably detect the burn scar with a size larger than 2 km^2 but poorly for smaller burn scars [10]. At local scales, burn scars and burn severities have been quantified by comparing the Landsat normalized burn ratio (NBR) (a spatial resolution of 30 m) between pre- and postfires [14], [15].

Burned areas have also been directly estimated from active fire hotspots of a single satellite instrument. Basically, the approach is to linearly correlate burned areas to fire pixel counts retrieved from one of the AVHRR, SPOT, Advanced Thermal Scanning Radiometer, and MODIS instruments over a large spatial grid on a monthly time scale [16]–[18]. For example, the global burned-area products are generated from MODIS [18], [19] and AVHRR active fire counts [20]. Recently, a more advanced and sophisticated method uses the combination of subpixel fire size and fire duration from Geostationary Operational Environmental Satellite (GOES) data to calculate half hourly burned areas in near-real time [21]. This approach is more applicable for fire monitoring, fire risk assessment, air quality forecasting, and decision making. However, active fire detections from a single instrument commonly produce high omission errors, particularly for small fires. For example, the omission error of fire detections from GOES-East Imager is about 38% on average, which increases exponentially with

Manuscript received April 20, 2010; revised December 1, 2010 and April 1, 2011; accepted April 11, 2011. Date of publication June 27, 2011; date of current version October 28, 2011.

X. Zhang is with Earth Resources Technology, Inc., Laurel, MD 20707 USA, and also with the National Oceanic and Atmospheric Administration/National Environmental Satellite, Data, and Information Service/Center for Satellite Applications and Research, Camp Springs, MD 20746 USA (e-mail: Xiaoyang.Zhang@noaa.gov).

S. Kondragunta is with the National Oceanic and Atmospheric Administration/National Environmental Satellite, Data, and Information Service/Center for Satellite Applications and Research, Camp Springs, MD 20746 USA (e-mail: Shobha.Kondragunta@noaa.gov).

B. Quayle is with the Remote Sensing Applications Center, United States Department of Agriculture Forest Service, Salt Lake City, UT 84119-2020 USA (e-mail: bquayle@fs.fed.us).

Digital Object Identifier 10.1109/TGRS.2011.2149535

0196-2892/$26.00 © 2011 IEEE

the decrease of fire sizes [22]. Similarly, more than 50% of small fires are undetected from MODIS in Brazil, Africa, and Eurasia [22]–[25]. In the U.S., the probability of small fire events undetected is more than 50% from the combination of Terra and Aqua MODIS (burned area < 1.05 km^2), from Aqua MODIS (burned area < 1.95 km^2), and from Terra MODIS (burned area < 3.34 km^2) separately [4]. The detection rate varies with time period and location of samples [4]. Generally, MODIS, with its superior spatial resolution and radiometric precision, detects much more small fires than GOES, while the high frequency of GOES observations (30-min interval) is able to capture either some fires with short duration or some fires obstructed by clouds during MODIS overpass [22], [26]. Using multiple satellite data in active fire detections compensates for the limitation of individual sensors [27].

Although several data sets of burned areas have been developed at regional and global scales using either satellite active fire counts or burn scars, the results are different substantively, and the accuracy remains problematic and is not well verified [6], [11], [28]. This paper investigates burned areas by blending all active fires identified from National Oceanic and Atmospheric Administration (NOAA) AVHRR, Terra+Aqua MODIS, and GOES (East and West) Imager. Specifically, burned areas are calculated from fire duration and fire size within a GOES pixel footprint. The fire duration is determined using instantaneous fire observations from MODIS, AVHRR, and GOES instruments. The fire size for GOES fire detections is obtained from the GOES fire product, while the size for MODIS and AVHRR observations is derived from the regression between fire hotspot counts and burned area from Landsat Thematic Mapper/Enhanced Thematic Mapper plus (TM/ETM+) imagery. The burned areas are then produced across contiguous United States (CONUS) during the period from 2004 to 2007. Finally, the results are extensively evaluated and validated for different ecosystems and burn scar sizes using both national inventory data and TM/ETM+-based burn scars.

II. Data Sets

The data used in this paper cover CONUS. The active fire hotspots detected from MODIS, AVHRR, and GOES Imager between 2004 and 2007 are used to estimate burned areas. The actual burned areas in 2005 that are derived from Landsat TM/ETM+ imagery and from National Fire Inventory (NFI) data are used to train the algorithm and to evaluate and validate the results separately.

A. Active Fire Data

Active fire counts from 2004 to 2007 are acquired from the Hazard Mapping System (HMS). HMS is an operational system for detecting fire and smoke in real time. It was developed in 2001 by the National Environmental Satellite, Data, and Information Service (NOAA NESDIS). This system generates a quality-controlled fire product after human analysts screen automatic fire detections from two geostationary and five polar orbiting environmental satellites [29]. Automatically detected fire products from GOES, MODIS, and AVHRR are provided at the ftp site (http://satepsanone.nesdis.noaa.gov/FIRE/fire.html). This product is validated and demonstrated to be generally reliable and satisfactory for CONUS [30].

Geostationary imagers on both GOES-12 (East) and GOES-11 (West) offer observations with a nominal spatial resolution of 4 km at satellite subpoint. The GOES-12 Imager scans the surface of South America and North America (excluding Alaska) at 15 and 45 min in each hour, while GOES-11 scans the west part of North America and the west coast of South America at 0 and 30 min. Over CONUS, the fire detections from GOES-12 in the western regions are affected by large view angles, while GOES-11 mainly detects fires in the western CONUS. Thus, we combined these two satellite observations to investigate burned area every 30 min. The WildFire Automated Biomass Burning Algorithm (WF_ABBA) identifies hotspot pixels from the 3.9-μm band. Then, GOES WF_ABBA derives instantaneous fire size and temperature based on a modified version of the Dozier bispectral method [31], [32]. In the Dozier algorithm, fire size and temperature are solved using two nonlinear equations which consist of radiances from the 3.9- and 11-μm bands and an estimate of the background nonfire pixel temperature [33]. The GOES fire product contains the time of fire detection, fire location in the latitude and longitude, instantaneous subpixel fire size, corresponding ecosystem type, and quality flag. The flag represents the confidence of fire detections with six different levels [32]. Specifically, the processed fire pixels (flag 0) are referred to as instantaneous fire observation from which subpixel fire size is calculated. These are the pixels that are not contaminated by clouds, and they do not cause sensor saturation, allowing for the estimation of subpixel fire size. This category accounts for about 38% of the fire observations according to data from 2002 to 2005 across CONUS [21]. The detected fire pixels with saturated, cloudy, moderate, and high probabilities are denoted with flags 1–4, respectively, for which fire size is not calculated. These categories account for about one-third of the fire observations. The rest of the fire detections are of low probability (flag 5), which could be false detections.

Polar orbiting fire observations for this study period are provided by the MODIS instruments on both the National Aeronautics and Space Administration (NASA) Terra and Aqua spacecrafts and the AVHRR on NOAA-15/17/18. These data provide a nominal spatial resolution of 1 km. Each instrument scans a surface location twice a day in low-middle latitudes. The Terra and NOAA-17 spacecrafts cross the equator near 10:30 A.M./P.M. local standard time (however, the NOAA-17 3.9-μm band does not operate during daylight), while Aqua and NOAA-18 do so near 1:30 A.M./P.M. NOAA-15 provides coverage near 6:00 A.M./P.M. The instruments on these satellites are used to automatically detect fire hotspots. Fires from AVHRR data are retrieved using Fire Identification, Mapping, and Modeling Algorithm [29], [34]. Basically, it uses the midinfrared band (3.55–3.93 μm) to identify all potential fires, uses the thermal band (10.3–11.3 μm) to eliminate clouds, has multiple filters for noise in the data, and uses the difference between brightness temperatures in the midinfrared and thermal bands to isolate fires from warm background. Similarly, MODIS fire detection is also based on various thresholds [35].

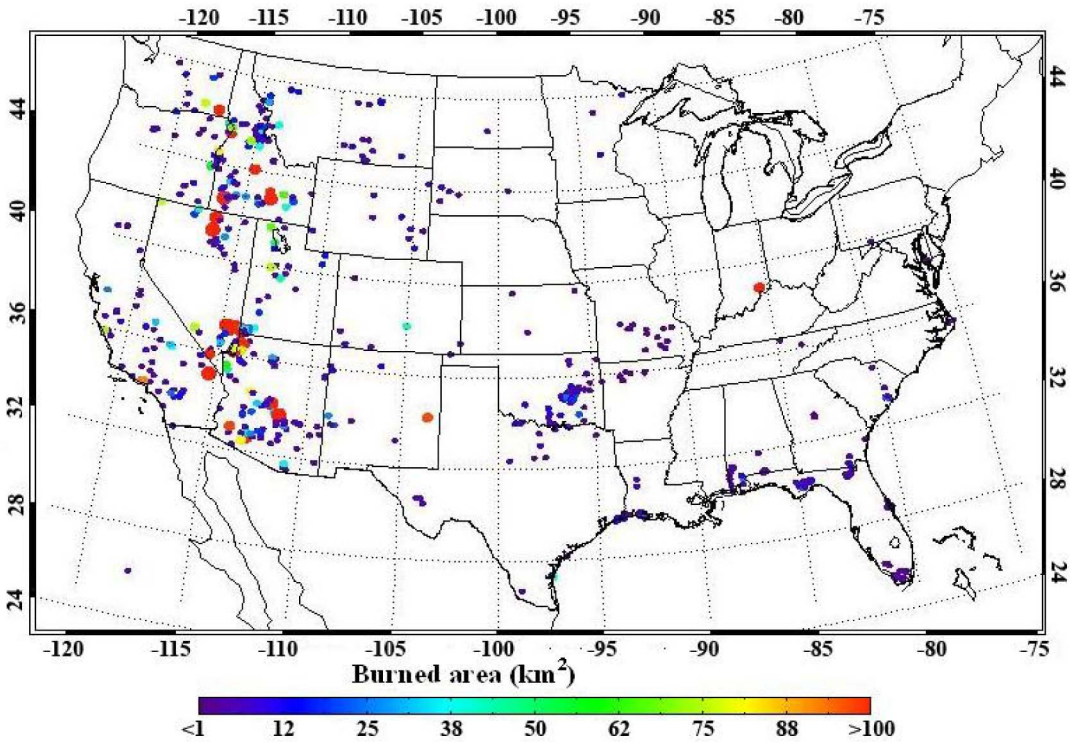

Fig. 1. Spatial pattern of burn scars in 2005 derived from TM/ETM+ data (the original data are obtained from http://www.mtbs.gov/). Note that the size of the dots is large for big burn scars for visualization purposes.

The HMS system allows satellite analysts to manually integrate fire data from all of the aforementioned satellite detections [29]. The analysts inspect fires detected from all instruments, delete detections that appear to be false alarms, and add fires that are undetected in the automated algorithms.

B. TM/ETM+-Based Burn Scars

Burn scars derived from Landsat TM/ETM+ imagery (30 m) represent the actual burned areas with high quality [36]. The Monitoring Trends in Burn Severity (MTBS) project (http://www.mtbs.gov/) is an interagency effort that is conducted jointly by the United States Department of Agriculture Forest Service and the United States Geological Survey. It calculates burned areas and burn severities for the historical fire events where TM/ETM+ data are available before and after fire occurrences [37]. Specifically, the process of developing burn severity from TM/ETM+ imagery is dependent on the differenced NBR (dNBR) data, a relativized dNBR (RdNBR), and the analyst interpretation. The analyst evaluates the dNBR and RdNBR data range and determines where significant thresholds exist in the data to discriminate between severity classes. The analyst is also aided by raw and pre- and postfire satellite imagery, plot data, and analyst's experience [37]. As a result, the MTBS project derives area-based burn severity in six possible thematic categories, which are unburned-low (containing areas of understory burn and/or very low severity burn that cannot be detected by satellite), low, moderate, high, increased greenness, and nonprocessing area mask (mostly cloud cover) [5], [14], [15]. The total area within the fire scar is equal to the area of the six thematic severity classes for each fire event. This data set also provides the ignition dates of fire occurrences for the selected fire events. For this paper, 522 burn scars from fire events in 2005 are collected from the MTBS data set (Fig. 1).

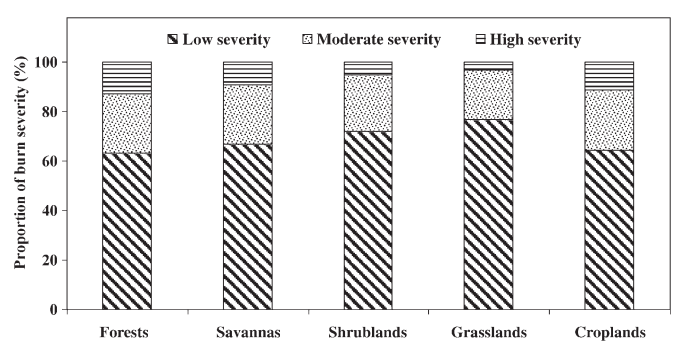

Fig. 2. Proportion of each burn severity from MTBS data in various ecosystems which are determined based on MODIS land cover type.

The actual burned area within a fire scar is determined by summing pixels that are classified as low, moderate, and high severities after nonprocessing area is allocated to other categories based on their areal proportions. The nonprocessing area is due to the cloud cover and the line drop errors over the TM/ETM+ burn scars, which accounts for about 6% of the areas over the samples. Among the actual burned area, the majority area is of low severity, which accounts for 69%, while the portion of moderate (23%) and high severity (8%) is much smaller. However, the proportion of different severities varies with the ecosystems, where low severity is highest in grasslands (Fig. 2) because the effects of long-term ecological burn severity to grassland areas are very minimal and because

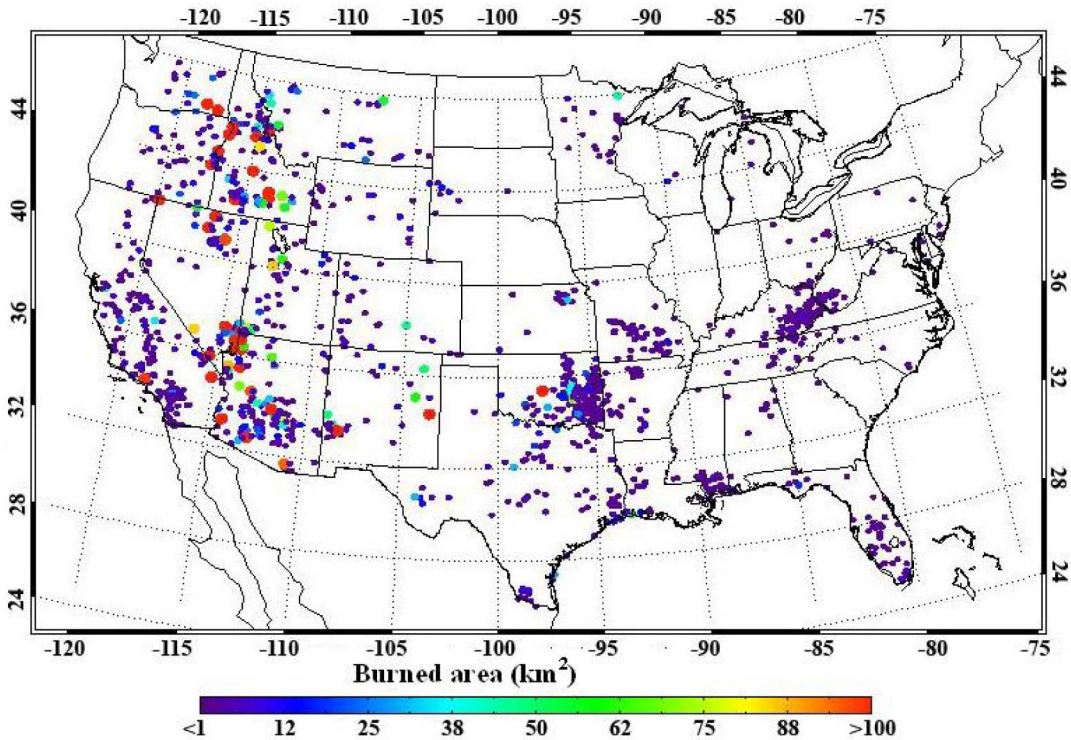

Fig. 3. Spatial pattern in burned areas from NFI in 2005. Note that the size of the dots is large for a big burned area for visualization purposes.

the grassland cover type is generally recovered by the peak of greenness of the next growing season. The proportion of unburned-low area within a fire scar is considerable. It is, on average, 40% and 35% for the fire events where the area within a fire scar is less than 1 and < 10 km^2, respectively. The unburned-low area is generally less than 20% for burn scars larger than 200 km^2. Indeed, if the unburned-low areas were not removed within the fire scar, the actual burned areas would be greatly overestimated. This would induce substantive uncertainties in algorithm training and validation for the area estimates from moderate-resolution satellite data.

C. NFI Data

Burned areas and fire occurrences in the NFI data are ground measurements which are reported from federal, state, and local agencies. The NFI data set in 2005 is obtained from the 2005 Incident Status Summary (ICS-209) reports (Fig. 3), which are from the National Fire and Aviation Management Web Applications site [38]. These reports contain about 2900 fire events with ground-based measurements, including fire location, size, and other information, but these fires only cover parts of fire events over CONUS. The burned areas are reported for the fire events in Wildland Fire Use, the wildland fires in confinement strategy, and other significant events on lands under federal protection or federal ownership, whereas the prescribed fires are not included. In the ICS-209 data set, burned area is small (which could be as small as 0.002 km^2) for the majority of the fire events, which is less than 1 km^2 in 40% of the events and less than 10 km^2 in 85% of the events. Note that the common mistakes in the ICS-209 data set include errors in the latitude and longitude, incorrectly reported complex fires, and actual burned areas [38]. For example, some of the fire events in the data set only last one day, but the reported burned areas are larger than 100 km^2. Thus, this data set is used for the general assessment of the burned area estimated from multiple satellite observations instead of accurate validation.

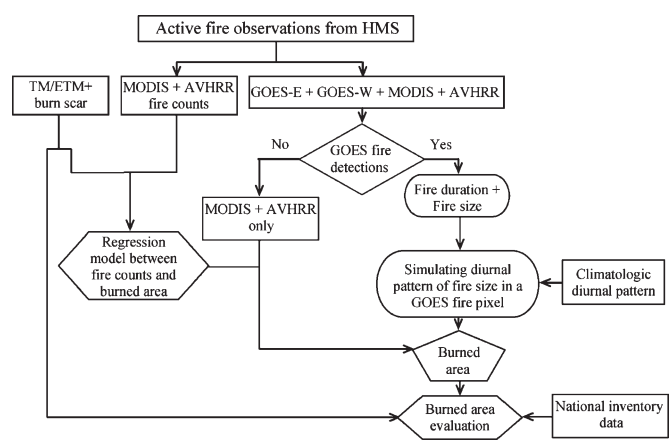

Fig. 4. Flowchart of integrating various satellite data for the estimates of burned area. MODIS+AVHRR active fires consist of detections from MODIS instruments on both the Terra and Aqua spacecrafts and AVHRR on the NOAA-15/17/18.

III. Methods

To estimate burned area, we analyze active fire observations from multiple satellite instruments. The general methodology of data processing is summarized in Fig. 4 and is described in detail in the following sections.

A. Simulating Burned Area Using Fire Size and Fire Duration From Multiple Instruments

Burned area is theoretically a function of fire duration and spread rate. Because fire spread rate is currently not feasible to derive from satellite observations, an algorithm using fire size and fire duration has recently been developed to estimate burned areas [21]. This method was tested using fire observations from GOES-East, in which some instantaneous fires were undetected. This paper uses the same algorithm but employs all of the fire detections from HMS (including MODIS and AVHRR) and GOES WF_ABBA. Briefly, burned area is assumed to be a function of instantaneous fire size and fire duration in the following empirical formula [21]:

$$A = \alpha \int_{t_s}^{t_e} F_t \, dt \tag{1}$$

where A is the area burned (in square kilometers) within a specified time period, F_t is the instantaneous subpixel fire size (in square kilometers), t_s and t_e represent the starting and ending times of a fire at an interval of half hour, and α is a coefficient of conversion (per half hour). The time step is set to half hour in this equation to match the temporal resolution of GOES satellite fire detections.

The coefficient α needs to be determined to convert fire size to burned area. The comparison between actual burned areas from TM/ETM+ burn scars in CONUS and GOES-East fire sizes in 2002 reveals that α could vary from 0.92 to 1.04 for the simulated half-hourly fire size, and the optimal value of α is 1.002 half-hour^{-1} [21]. This suggests that the simulated half-hourly fire size is equivalent to the burned area if the diurnal pattern of fire duration is simulated properly. Thus, the optimal value of α is adopted for the burned-area estimates in this paper. In order to reduce uncertainty which may occur in data processing, the total burned area in a fire pixel is not allowed to exceed the individual GOES pixel size, which is 4 km by 4 km at nadir.

To calculate burned areas, the diurnal variation in fire characteristics is reconstructed for a given fire pixel from multiple satellite instruments. First, fire size and time (UTC time) within a day are integrated from multiple satellites for individual GOES fire pixels. The fire size in every half hour (0–29 and 30–59 min) is determined from GOES instantaneous fire sizes [39], [40]. If GOES-East and GOES-West both calculate instantaneous fire size within a half hour for a given fire pixel, the average fire size is used. Otherwise, fire size is selected from the one which provides the valid value. If the fire detections from both GOES-East and GOES-West do not provide fire sizes, only the time is recorded for the determination of fire duration. Furthermore, the time of the instantaneous fire observation is also obtained from all fire detections of MODIS and AVHRR within a GOES pixel. Because the fire size for MODIS and AVHRR fire detection is not calculated, it is treated in two different ways. If there are GOES fire detections within a day, MODIS and AVHRR fire detections are only used to improve the quality of fire duration in the corresponding GOES fire pixel. Otherwise, the fire sizes of MODIS and AVHRR fire counts are obtained from the regression model (MODIS+AVHRR fire counts against the actual burned area) in different ecosystems, which is discussed in Section III-C.

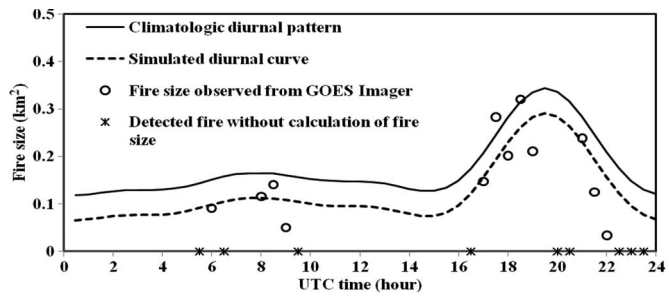

Fig. 5. Example in simulating the diurnal pattern of fire sizes from available fire sizes observed in a GOES pixel. The fire sizes are obtained from the GOES WF_ABBA product, while the observations without fire sizes, denoted using asterisks, are from the MODIS+AVHRR+GOES data. This example is obtained from shrubland fire in the western CONUS in July 2005.

Second, the method developed in [21] is applied to simulate diurnal pattern of fire size from the recorded half-hourly fire sizes and fire durations. Briefly, the climatologic diurnal patterns in half-hourly GOES fire sizes were generated from all of the fire sizes for forests, savannas, shrublands, grasslands, and croplands (croplands plus cropland/natural vegetation mosaics, which are used in the following context), respectively, using GOES-East fire observations from 2002 to 2005 across CONUS [21]. Assuming that the shape of the diurnal pattern in a given ecosystem is similar, the diurnal curve of fire sizes for a given pixel is then generated by imposing the corresponding climatologic diurnal curve on the detected fire sizes (Fig. 5). The overall absolute mean difference between the simulated value in the diurnal pattern and the original GOES fire size in 2005 is about 0.1 km^2, and the mean bias error is 0.007 km^2. In this way, the magnitude of the calculated fire sizes for an individual pixel is generally controlled by the actual satellite observations. From the fitted curve, fire sizes are obtained for those fire observations where the fire size is not calculated: the detected GOES fires which are saturated or contaminated by clouds, the MODIS+AVHRR detections, and the missed detections. Finally, the burned area is estimated from the simulated diurnal pattern using (1).

Some of the fire detections are not considered for the estimates of burned area. First, a fire pixel is only observed from GOES Imagers (not AVHRR or MODIS) with low probability (quality assurance flag 5) and for less than three times a day. Second, a fire within a GOES pixel footprint is only observed once a day by either MODIS or AVHRR but not by GOES. These fires could be either false detections or very small fires. Very small fires could lead to great overestimation of burned areas [43].

B. Matchup of Satellite Hotspots With Burn Scar Data

In order to determine the relationship between burned area and MODIS and AVHRR fire counts and to evaluate and validate the burned-area estimates from active fire observations, the pixels of active fires from MODIS, AVHRR, and GOES Imager instruments are separately matched with burned areas in both TM/ETM+-based burn scars and national inventory data in 2005. The matchup takes into account both time and

space. First, because the starting and ending dates of a fire event may not be accurately recorded in the field, these dates are extended for ten days for the calculation of the active fire counts from multiple satellites. This extension will not cause the overestimation of the total fire counts because there will be no hotspots if there are no fire occurrences. Second, the geolocation between burn scar coverage and active fires are further matched. Assuming the burn scar coverage initially to be a circle where the area is obtained from either national inventory data or MTBS project, the radius (r_a) is then used to determine the relative latitude and longitude of the scar boundary based on the following formula.

The difference of the longitude (δ; in degrees of arc) for a burn scar is

$$\delta = 2r_a/Rcos\phi \tag{2}$$

where ϕ is the latitude (in degrees), r_a is the radius of the burn scar (in meters), δ is the difference of the longitude (in degrees of arc), and R is the radius of the earth $(6.3711 \times 10^6$ m).

The difference of the latitude ($\Delta\phi$ in degrees of arc) for a burn scar is

$$\Delta\phi = 2r_a/R. \tag{3}$$

Satellite fire hotspots are calculated for a given fire event after the time period and geolocation are matched. In particular, the fire observations within the latitude $(\Delta\phi)$ and longitude (δ) bounds are counted from GOES, MODIS, MODIS+AVHRR, and MODIS+AVHRR+GOES, respectively. Because the spatial coverage of an actual burn scar is irregular, the fire observations in a given period are also calculated from a series of buffer zones of $2r_a, 3r_a, \ldots$, and $10r_a$, in turn. Generally, fire counts increase with the enlargement of the buffer zone. The final fire counts for a given burn scar are determined once the rate of increasing counts reaches the first minimum with increasing buffer zone. In other words, the buffer zone varies for individual fire events. Furthermore, the matched data of burned areas and fire counts are stratified based on MODIS land cover types, which are forests, shrublands, savannas, grasslands, and croplands (including cropland and natural vegetation mosaics) [44]. The MODIS land cover at a spatial resolution of 1 km (collection 4) is downloaded from NASA (https://wist.echo.nasa.gov/api/).

C. Determination of the Burned-Area Rate in an Active Fire Count

Because fire size is not provided in AVHRR and MODIS fire products, the rate of burned area (in square kilometers per fire count) in a satellite fire count is derived by comparing the corresponding fire counts with TM/ETM+-based burn scars which provide reliable actual burned areas. The focus here is to explore the burned-area rate for a small amount of fire events that are only detected from MODIS and AVHRR but not from GOES. In these cases, fire events are generally small. To do this, the fire counts are linearly correlated to TM/ETM+-based burned areas as the intercept is set to zero and as the confidence level is set to 95%. Because samples with a large burned area strongly control the linear regression slope, which may result in poor representation for small fire events, the regression is established using all burn scars, with the burned areas less than 160 km^2, no matter whether the scars were detected from GOES or not. As a result, 162 burn scars in forests and 263 burn scars in nonforests are used to establish regression separately. The slope of the linear regression is taken as the rate of the burned area in a fire count (Fig. 6). The rate is calculated for forest and nonforests. The nonforest category is not further stratified for the establishment of regression models because the samples are small and scattered for croplands and savannas. Note that this analysis takes all fire observations (including multiple observations for a MODIS or AVHRR pixel) in a burn scar into account because it is assumed that more observations represent longer fire duration and larger burned area. Moreover, large fire events (burned area > 160 km^2) are excluded because samples with large burned area strongly control the linear regression slope, which may result in poor representation for small fire events.

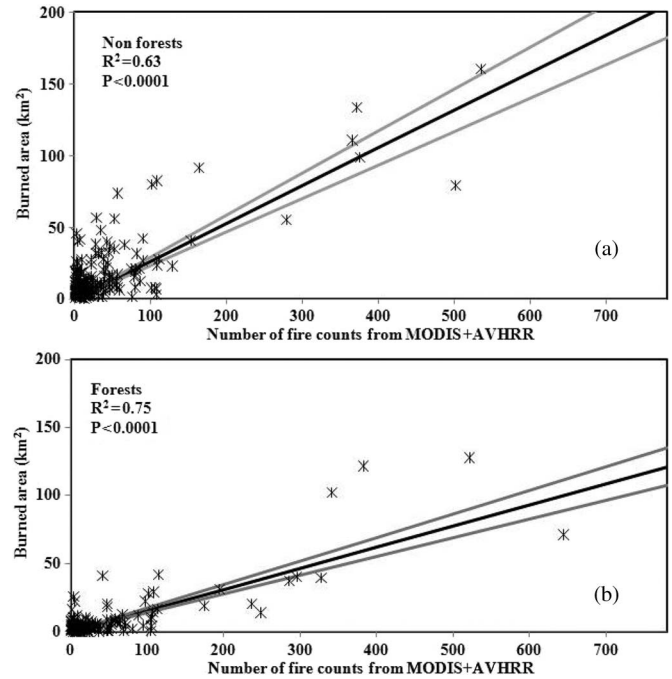

Fig. 6. Scatter plot of the burned areas of active fire hotspots from MODIS+AVHRR against TM/ETM+-based burn scars. The dark line is the ordinary least squares linear best-fit passing through the origin, and the grey lines are the 95% confidence intervals on the mean. (a) Nonforest fires. (b) Forest fires.

As expected, active fire counts increase with the size of TM/ETM+-based burn scar. The correlation between burn scars and active fire counts is significant ($p < 0.0001$; Table I). The burned-area rate in each MODIS observation is 0.351 km^2 for the total area (including unburned area) within a fire perimeter, while it is 0.288 km^2 for the actual burned area (low-high severities). However, the rate of moderately-highly burned area is much smaller. The rate from MODIS+AVHRR observations is 0.212 and 0.204 km^2 for the total and actual burned areas, respectively. Moreover, the rate is generally larger in nonforest fires than in forest fires and varies with burn severity (Table I). In the final estimates of burned area, this paper uses the rate of actual burned area per MODIS+AVHRR count.

TABLE I
RATE OF BURNED AREA (IN SQUARE KILOMETERS) FOR EACH ACTIVE FIRE OBSERVATION FROM MODIS AND AVHRR($P < 0.0001$), WHICH IS DERIVED BY COMPARING MODIS AND MODIS+AVHRR FIRE COUNTS WITH TM/ETM+ BURN SCARS SEPARATELY. NOTE THAT GOES FIRE OBSERVATIONS ARE NOT INCLUDED

	MODIS		MODIS+AVHRR	
	Forests	Non forests	Forests	Non forests
Total area within burn scar perimeter	0.350	0.350	0.183	0.280
Low-highly burned area	0.265	0.301	0.155	0.263
Moderately-highly burned area	0.124	0.129	0.064	0.067

The burned areas and fire counts in some samples do not match well because satellite observations are limited in some fire events due to cloud covers, tree canopy, viewing angle, and other factors. This suggests that the burned areas estimated directly using active fire counts are of high uncertainty. Therefore, this paper uses this regression approach to determine burned area only for fires that are not observed by GOES Imager, particularly for small fires. For example, when comparing with the national inventory data in 2005, among the fire events detected by satellites with burned area less than 1, 1–10, and 10–20 km^2, the proportion of fire events only detected by MODIS+AVHRR (without GOES) is 74%, 44%, and 13%. The corresponding proportion of total burned area for these three categories is 1.5%, 11.86%, and 7.8% separately. In other words, there is a limited burned area that is only detected by MODIS+AVHRR but not by GOES.

D. Evaluation Approach

Evaluation is conducted using both higher spatial resolution remote sensing data (TM/ETM+) and ground-based measurements (NFI ICS-209) to quantify the accuracy of estimates from MODIS+AVHRR+GOES instruments. Note that TM/ETM+-based burn scars are also used for validation. It is because only 163 among 522 burn scars are calculated using the regression approach with fire counts, as shown in Section III-C, while others (359) are calculated from simulated diurnal pattern of fire size (described in Section III-A), although 162 samples in forests and 263 samples in nonforests are used to train the burned-area rate in active fire counts.

Previous studies validated the estimates of burned area after aggregating the data to 0.33°–1.0° grids over a large coverage [21], [28]. Such comparison generally eliminates the uncertainties in the estimates of individual burn scars. Alternatively, this paper compares each individual fire event in 359 of TM/ETM+ burn scars and 2900 of NFI ICS-209 data. The evaluation process consists of two parts. First, the detection rate of fire events from multiple satellites is evaluated to verify the quality of fire observations. The factors influencing fire detection rate are further examined by associating them to burn severities and burn scar sizes. Second, the accuracy of burned area estimated from MODIS+AVHRR+GOES is investigated for various ecosystems and burn scar sizes. In particular, individual fire events obtained from TM/ETM+-based burn scars and national inventory data are stratified into five different ecosystems and 11 categories of burn scar sizes for accuracy assessments.

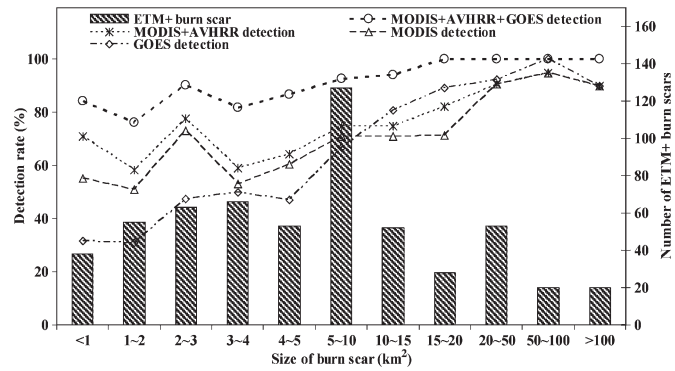

Fig. 7. Detection rate of TM/ETM+-based burn scars from multiple satellite instruments. The detection here indicates that a fire event is observed by satellites at least once. The right y-axis indicates the number of TM/ETM+ burn scars, and the left y-axis indicates multiple satellite detection rates.

IV. RESULTS

A. Evaluation of the Burned Area Estimated From Active Fire Observations

1) Comparison With TM/ETM+-Based Burn Scars: Multiple satellite sensors detect most fire events at least once as each TM/ETM+-based burn scar is taken as one fire event in 2005 (Fig. 7). GOES Imager detects more than 80% of fire events with a burn scar larger than 10 km^2, which is higher than those from MODIS and MODIS+AVHRR. This is likely associated with the fact that the high frequency of GOES observations would capture fires in a short cloud-free period, while MODIS and AVHRR observations could be obstructed by cloud cover. Nevertheless, for small fire events with burn scars less than 1, 5, and 10 km^2, the detection rate from GOES Imager is 32%, 43%, and 50%, respectively, while from MODIS, it is 55%, 59%, and 63%, correspondingly. The detection rate using MODIS+AVHRR instruments is 6%–16% higher than that using MODIS alone. In contrast, MODIS+AVHRR+GOES detects 87% of the small fire events (< 10 km^2). This rate is 18%, 24%, and 36% higher than that from MODIS+AVHRR, MODIS, and GOES separately. The multiple instruments detect all fire events with an area larger than 15 km^2. Among the undetected fire events, 67% are low severity fire events without any moderately and highly burned areas within the perimeter of the burn scars. It is likely that low severe fires release a limited fire energy, making it hard for satellites to discriminate hotspots from warm background. Some other undetected events are likely associated with the obstacles of clouds and canopy cover, the resolution and view angle of satellites, and the heterogeneity of the surface.

The burned areas derived from multiple satellite active fires in 2005 are correlated well with TM/ETM+-based burn scars across CONUS (Fig. 8). The root-mean-square error is 14.1 km^2 for all of the samples. The linear regression (at 95% confidence) intercept is $-0.92 \pm 0.64 (P = 0.152)$, and the slope is 1.0288 $\pm$ 0.0079 ($P < 0.00001$). This indicates that the samples of burned-area estimates against TM/ETM+-based burn scars are generally distributed along a 1:1 line, which means that there is no significant systematic bias. At ecosystem levels, the regression slope is larger than 0.9, except

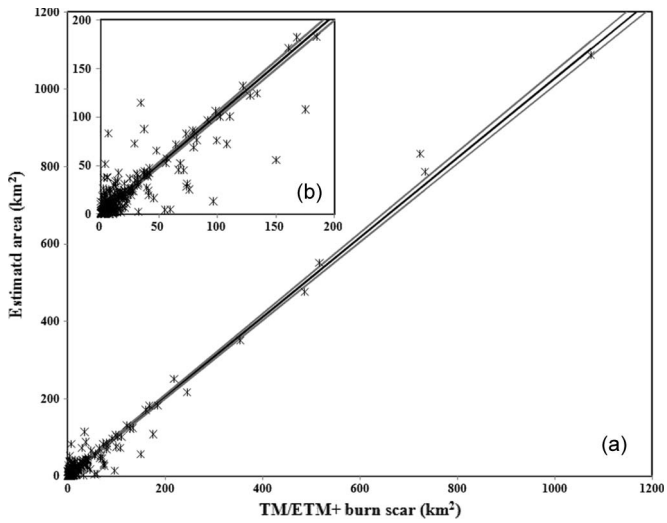

Fig. 8. Comparison of burned areas estimated from MODIS+AVHRR+GOES active fires, with burn scars derived from TM/ETM+ imagery in 2005. The dark line is the ordinary least squares linear best-fit passing through the origin, and the grey lines are the 95% confidence intervals on the mean. (a) Scatter plot for all samples. (b) Plot presenting the pattern for samples with small burned area (less than 200 km^2).

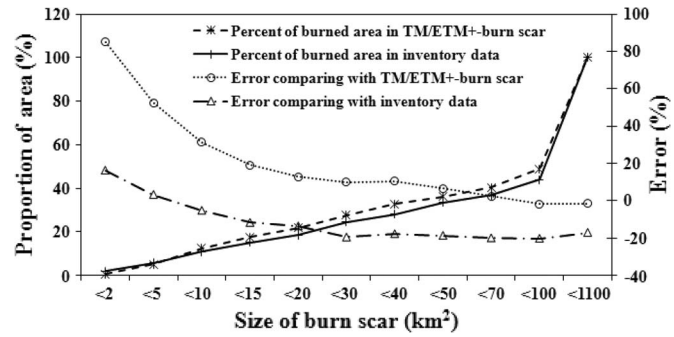

Fig. 9. Variations in both estimation accuracy and percentage of burned area with the size of TM/ETM+ burn scar coverage and national inventory in 2005 separately. Note that both percentages of area (left y-axis) and error (right y-axis) are based on the cumulative size of the burn scar.

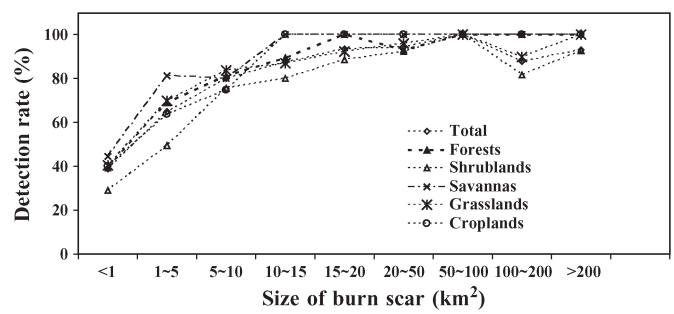

Fig. 10. Variation in the proportion of fire events detected from MODIS+AVHRR+GOES with sizes of burned areas from NFI data in 2005.

for savannas where the slope is 0.73. The determination of correlation (R^2) indicates that the estimated area explains more than 80% of the variation in TM/ETM+-based burn scars for each individual ecosystem, which does over 97% in forests and shrublands, respectively.

The accuracy of the burned-area estimates varies with the ecosystems. The burned area is slightly overestimated in forests and savannas, with an error of 13% and 30%, respectively. However, it is underestimated in shrublands (2.2%), grasslands (8.4%), and croplands (15.7%). These errors are likely associated with the fire energy released from fires. In forests and savannas, a large amount of fuel loadings usually causes intense and severe fires, which are easy to be detected from satellites. In contrast, fires are of relatively low intensity in shrublands, grasslands, and croplands where the small amount of fuel loading is available [45]. Thus, the fires with less radiative energy are relatively hard to be continuously observed.

Burned areas are well estimated in large fire events but poorly in small fire events (Fig. 9). The error of estimate, which is the difference between the estimated value and the TM/ETM+ measurements divided by the TM/ETM+ measurements after they are aggregated over a particular burn scar size group, decreases exponentially with the increase of burn scar size. Burned area is almost overestimated by 85% for the burn scars less than 2 km^2. However, the areas are estimated properly (accuracy $> 70\%$) for the burn scars larger than 10 km^2. The accuracy is larger than 90% for the burn scars larger than 30 km^2. Compared with all of the TM/ETM+-based samples in 2005, the total burned area estimated from MODIS+AVHRR+GOES active fires $(1.16 \times 10^4$ km$^2)$ is equivalent to the areas in TM/ETM+-based burn scars $(1.18 \times 10^4$ km$^2)$. The overall accuracy is 98.9%. This is better than the burned areas estimated from GOES alone, where the overall accuracy is 82%. The high overall accuracy from MODIS+AVHRR+GOES estimates suggests that the large errors in the burned-area estimates for small fire events play a very minor role in the estimates of total burned area in a regional scale. It is because the areal proportion is only 0.67% and 12.4% for the fire events less than 2 and 10 km^2, respectively.

2) Comparison With National Inventory Data: The comparison of the satellite-derived burned area to the data from national inventory shows that the fire detection rate from multiple satellites is a function of ecosystems and the size of the burned area reported in national inventory data in 2005 (Fig. 10). The detection rate from MODIS+AVHRR+GOES is very similar in various ecosystems, except for shrublands. Overall, MODIS+AVHRR+GOES detects 40% of small fire events (burned area $<$ 1 km^2) in NFI ICS-209 and more than 80% of large fire events (burned areas > 10 km^2). For small fire events $(< 10$ km$^2)$, the detection rate from MODIS+AVHRR+GOES is 26%, 17%, and 7% higher than that from GOES, MODIS, and MODIS+AVHRR, respectively. This demonstrates that the detection rate from MODIS+AVHRR+GOES is greatly improved relative to detections of individual instruments. Except the impacts of low fire energy, cloud cover, and canopy cover, the undetected fire events are also likely associated with the errors of either the geolocations or dates of fire occurrences in the inventory data. In particular, the latitude and longitude in some fires are not provided so that the centroid coordinates of the county shape are written in the activity records [46]. Despite the large number of undetected small fire events, the related burned areas are less than 5% across CONUS.

The multiple satellite-based estimates of burned areas are matched well with the ICS-209 data in 2005. The comparison

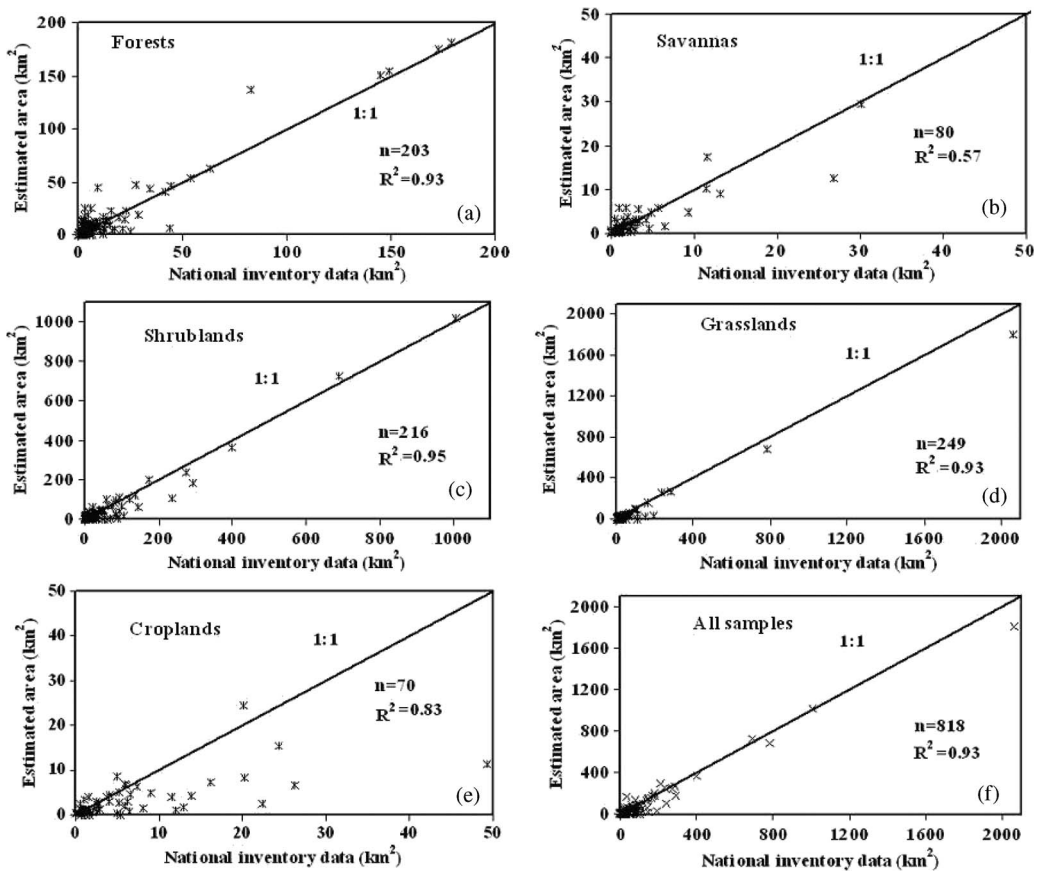

Fig. 11. Burned areas in individual fire events derived from multiple satellite hotspots against the NFI data in 2005.

of the matched fire events shows that the overall accuracy of the burned area estimated from the MODIS+AVHRR+GOES is 83%, while the accuracy from GOES alone is 70%. The satellite estimates are slightly smaller than the inventory data. This result is expected because uncertainties exist in both data sets. As reported by [46], the field measurements are difficult in large regions, and the national inventory data usually contain a certain amount of unburned areas (24% on average) within the fire's perimeter. If the proportion of unburned area is excluded from the national inventory data, the difference between these two data sets is much smaller.

The accuracy of the burned-area estimates varies with different ecosystems (Fig. 11). The satellite estimate of the total burned area in the forest fire events is about 30% higher than the national inventory data. However, it is relatively smaller than the inventory data in other ecosystems. The relative error of the burned-area estimate is 12%, 19%, 29%, and 25% for savanna, shrubland, grassland, and cropland fires, respectively. In other words, the accuracy in the total burned area ranges from 70% to 88% for individual ecosystems. The correlation coefficient (R^2) indicates that the satellite estimates can explain the variations in the inventory data, with a proportion of 92%, 95%, 57%, 93%, and 83% for forest, shrubland, savanna, grassland, and cropland fires, respectively.

This validation also indicates that the burned areas estimated from the MODIS+AVHRR+GOES active fires are overestimated in small fire events and underestimated in large fire events (Fig. 9). The error ranges from 17% (overestimates) to -20% (underestimates) for different sizes of burned areas in inventory data. This pattern is identical to the difference between the MODIS+AVHRR+GOES estimates and the TM/ETM+-based burn scars.

B. Spatiotemporal Pattern in Burned Areas

The spatial pattern in burned area is complex. The mean annual burned area across CONUS is $3.4 \times 10^4 \pm 0.7 \times 10^4$ km^2 from 2004 to 2007, which accounts for about 0.4% of the total land. As expected, the burned areas are mainly distributed in the western U.S., southeastern U.S., and along the central and southern Mississippi Valley. Large burned areas for fire events are dominantly distributed in the western U.S., where the areas could be larger than 200 km^2 in a 0.25° grid aggregated from individual GOES fire pixels (Fig. 12). However, small burned areas are densely distributed along the central and southern Mississippi Valley, which are generally associated with agriculture activities.

Burned area varies distinctively in different states across CONUS (Fig. 13). The area burned is large in CA, AZ, ID, and TX, which accounts for 15.5%, 9.4%, 8.8%, and 8.6% of the total burned area, respectively. In these states, the burned area is mainly caused by shrubland fires in CA and AZ, by grassland fires in TX, and by forest fires in ID. The proportion is less than 5% in other states. However, the burned area is also noticeable in the states along the Mississippi Valley. Specifically, it is over 1% of the total burned area in MO, AL,

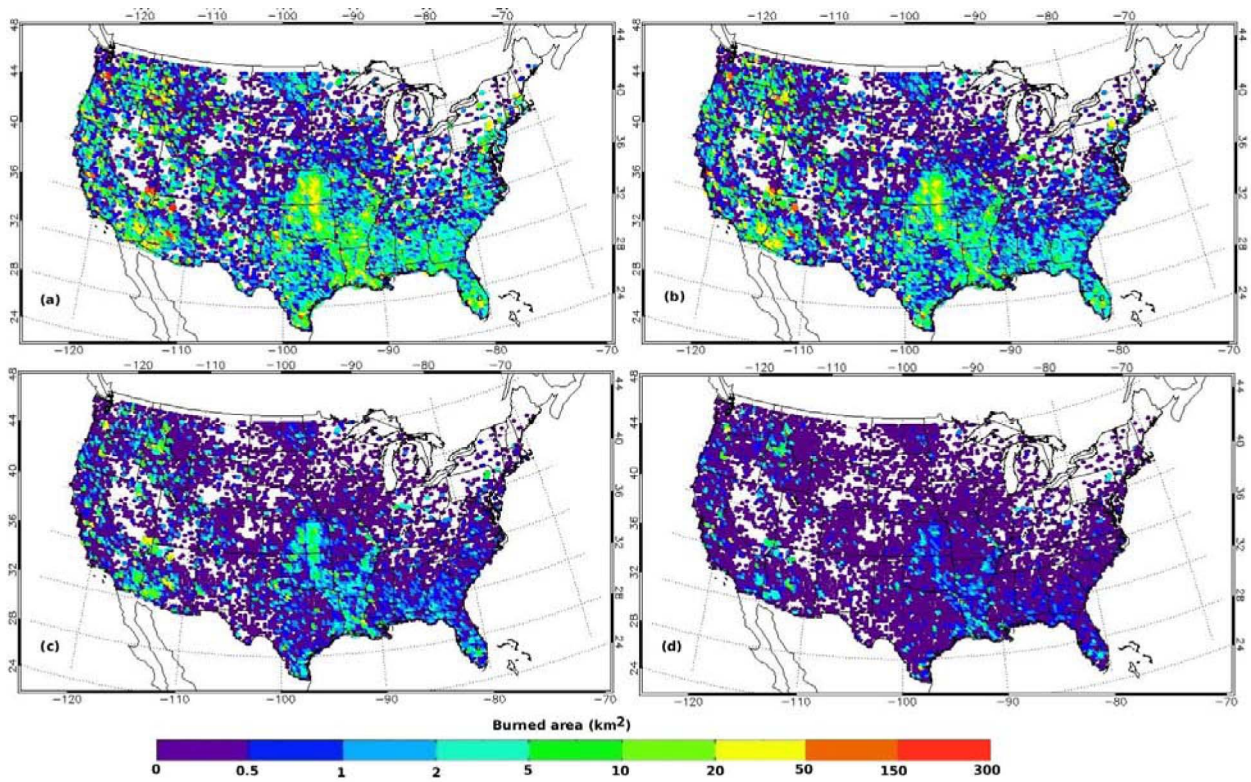

Fig. 12. Distribution of burned areas in 0.25° grids aggregated from GOES fire pixels (∼4 km), where the burned area is calculated from GOES+AVHRR+MODIS active fires in 2005. The area varies with the following different severities: (a) actual burned area, (b) low severity, (c) moderate severity, and (d) high severity. These spatial patterns in burn severity are extrapolated based on ecosystem-level allocation from MTBS data.

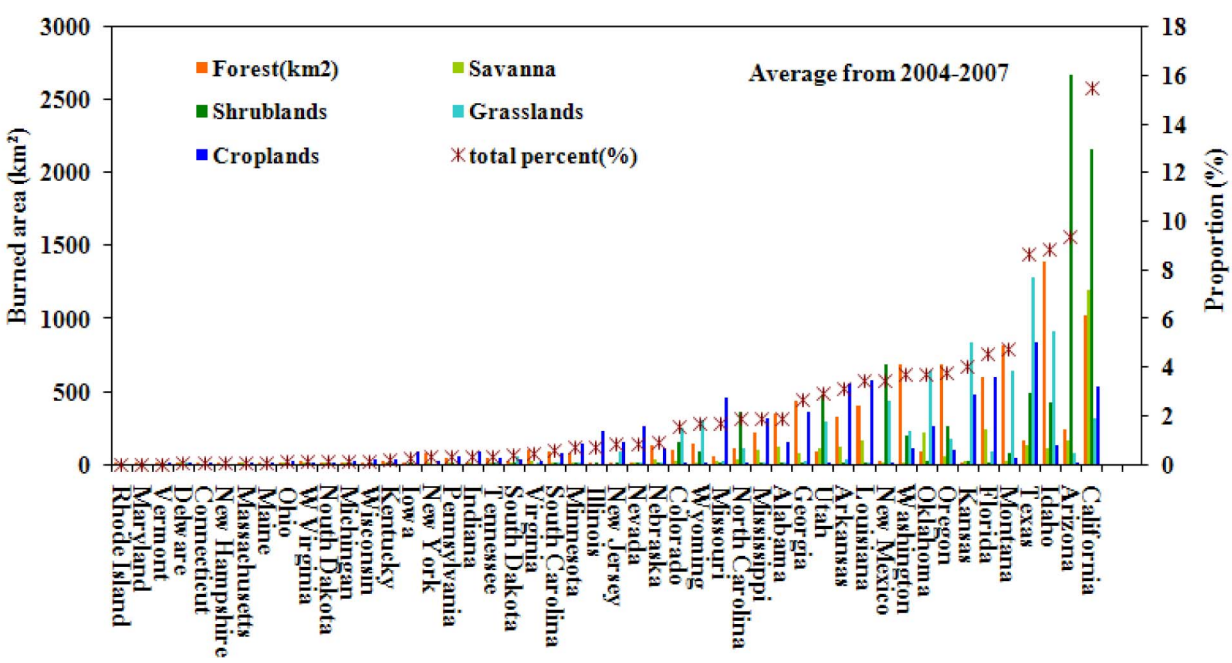

Fig. 13. Average burned area (2004–2007) for different states and ecosystems.

and MS separately. Moreover, the southeastern U.S. is another region with large burned areas. The proportion of burned area is 2.6% in GA and 4.6% in FL, where drier-than-normal conditions mainly cause severe wildfires during spring and fall, although lightning is responsible for wildfires in some years (Heilman *et al.*, 1998) [47].

The areas with different burn severities vary considerably [Fig. 12(b)–(d)]. These areas are allocated spatially from the total actual burned area according to the proportion of different severities in ecosystems described in Fig. 2. The area with low burn severity is largest, which presents a similar pattern to that of the actual burned area [Fig. 12(a)]. However, the burned area

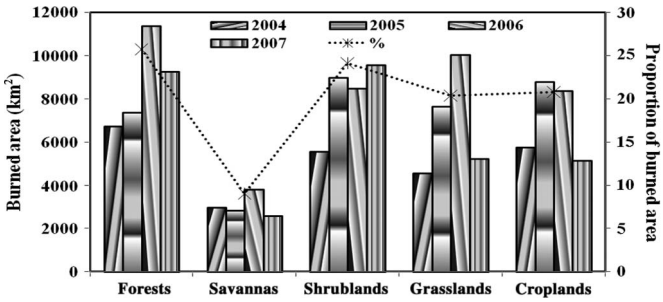

Fig. 14. Variation in burned area with ecosystem across CONUS. The dotted line on the right y-axis represents the average proportions of burned area from each ecosystem to the mean annual burned area over the CONUS between 2004 and 2007, and the left y-axis represents the burned area in individual years from 2004 to 2007.

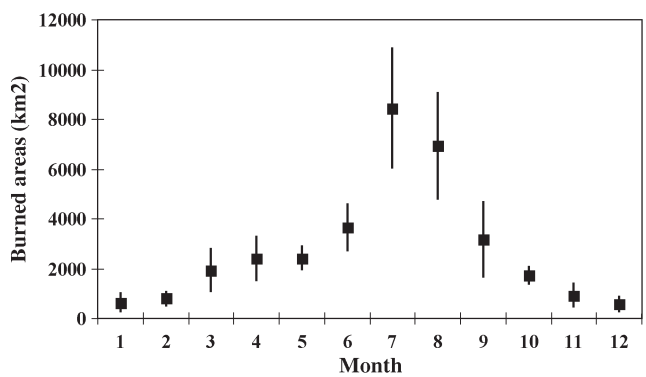

Fig. 15. Seasonal variation in monthly burned area averaged from 2004 to 2007 across CONUS. The squares indicate the mean value, and the bars represent the standard deviation.

with high severity is very small, which is generally less than 10 km^2 in a 0.25° grid. This implies that large areas with low burn severity emit limited trace gases and aerosol, which significantly affects the estimates of biomass burning emissions.

Burned area is also a function of ecosystem across CONUS (Fig. 14). The largest burned area appears in shrublands in 2005 and 2007, while it is largest for forests in 2004 and 2006. Among the total burned area during the four years, the area burned in forests and shrublands is about 25%, respectively, and it is 21% in grasslands and croplands, respectively. The area is always smallest in savannas. Nevertheless, compared with the total area of each individual ecosystem across CONUS, the proportion of area burned annually by fires is 0.49%, 0.64%, 0.68%, 0.40%, and 0.30% in forests, savannas, shrublands, grasslands, and croplands, respectively.

Burned area presents a remarkable seasonal pattern (Fig. 15). The area is 1.7×10^4 km^2 during July and August, which accounts for 46% of annual burned area. In contrast, it is 0.3×10^4 km^2 (9%) from November to next February. Evidently, the fire season across CONUS with the relatively largest area impacted is summer, although individual large fire events may occur in other months, such as the GA fire in May 2007 and the San Diego fire in October 2007. At state levels, the occurrence of the largest monthly burned area varies from April to September in the southeastern U.S., while it changes from June to August in the western U.S., respectively. This variation is likely associated with regional differences of climates and land management policies. For example, the burned area increases rapidly during summer in CA because of hot temperature and dry condition, and it is largest in April–May in FL because of limited precipitation. Agricultural fires, which are mainly distributed along the central and lower Mississippi Valley, present weak seasonality from April to September. It is likely because agricultural fires could be set during the harvesting, postharvesting, and preplanting periods for clearing crop residue, fertilizing the soil, and eliminating insects and disease from the fields [48].

V. Discussion and Conclusion

The results shown here have demonstrated that using multiple satellites enhances fire detections relative to individual instruments. Compared with the fire events described in TM/ETM+-based burn scars, MODIS+AVHRR+GOES instruments identify more than 87% of fire events with area less than 10 km^2 and almost all other larger events. This is 18% higher than the detections from MODIS+AVHRR, 24% higher than MODIS instruments, and 36% higher than GOES Imager. Nevertheless, the detection rate using MODIS+AVHRR+GOES is relatively low in comparison with the national inventory data in which geolocation errors exist in some fire events. It is about 40% of small fires (< 1 km^2) and more than 80% of large fire events (> 10 km^2). The undetected fires are mostly low severity fires and shrubland fires with low fire radiative energy, which play a minor role in biomass burning emissions. The high detection rate, especially compared with the burn scars from TM/ETM+ imagery, suggests that leveraging the combined spatial and temporal resolution of multiple polar and geostationary satellite observation platforms is a powerful tool in the detections of fire events. Note that the commission error of multiple satellite fire detections is not investigated in this paper because both TM/ETM+ burn scars and national inventory data do not include all actual fires across CONUS.

Considering the well-detected fire events from MODIS+AVHRR+GOES, the burned areas are effectively derived by combining subpixel fire size and fire duration. The results in this paper have indicated that the annual burned area is $3.4 \times 10^4 \pm 0.7 \times 10^4$ km^2 from 2004 to 2007. The burned area is dominantly distributed in CA, AZ, ID, and TX, which is followed by the states in the southeast region and along the Mississippi Valley. The annual fire events burn 0.4% of the total land across CONUS. This consists of 0.49% of forests, 0.64% of savannas, 0.68% of shrublands, 0.40% of grasslands, and 0.30% of croplands. These fire events are large in summer, although the month with the largest burned area varies with different states. Moreover, among the burned areas, the areas of high severity are small, while those of low severity are dominant.

Comprehensive evaluation demonstrates that the burned areas estimated from MODIS+AVHRR+GOES are reliable. The burned area is slightly overestimated in forests and savannas, while it is slightly underestimated in shrublands, grasslands, and croplands. The error in each ecosystem is generally less than 15% in comparison with TM/ETM+ burn scars. However, the error of the estimate ranges from 12% to 30% in different

ecosystems in comparison with the national inventory data. In addition, the burned areas are overestimated in small fires, particularly for a scar coverage less than 5 km^2, but the areas are well estimated for large fire events. The accuracy of the total burned area across CONUS is 98.9% for TM/ETM+-based burn scars and 83% for the national inventory data. This suggests that the large error in the area estimates for small fire events has little impacts on the estimates of the total burned area at a continental scale. However, the large uncertainty of burned area in agricultural fires, which are generally small, could impact the estimates of biomass burning emissions because of the relatively large fuel loadings compared with some shrublands and grasslands. The extensive evaluation and validation has also demonstrated that the algorithm using fire size and fire duration from multiple satellite data provides a robust tool in estimating burned areas. This can be applied in near-real time, which is particularly useful in qualifying biomass burning emissions for air quality forecasting.

Note that accurate simulation of the diurnal pattern of fire size is crucial in the estimate of burned area in this paper. This is dependent on the instantaneous subpixel fire size from the GOES WF_ABBA fire product. The calculation of the GOES instantaneous fire size using the Dozier bispectral method [31] has been conducted in various research during the last two decades [32], [33], [39], [42], and the results have also been evaluated [39], [40]. However, a sensitivity analysis indicates that the fire size estimates from the Dozier approach would produce large uncertainties [49]. Certainly, the GOES subpixel fire size needs to be validated thoroughly in the future to qualify the accuracy. Even so, it still provides valuable information for us to simulate diurnal pattern of fire size, although the detailed uncertainty of the simulation needs to be analyzed. The simulated value smoothes the irregular variation in raw fire size data and reduces the large uncertainties in individual detections. As a result, the diurnal pattern algorithm could produce reasonable estimates of burned area, particularly for large fire events.

The rate of burned area in a MODIS and AVHRR fire count is complex, and it should be used with caution. The relationship between the burned areas and active fire counts for small fire events is relatively noisy despite the strong correlation. It is due to the fact that fire counts vary greatly in the same size of burn scars because of the impacts of cloud, canopy cover, low fire energy, and other factors. Generally, the rate of burned area in a fire count is controlled by a few samples with a large burned area. However, the small burned area in the majority of the fire events is poorly represented. Thus, using a single rate to calculate the burned area from satellite fire counts would produce high uncertainties. In a continental scale, the burned area in the majority of fire events is less than 1 km^2, which account for less than 10% of the total burned area. For example, the national inventory data set in 2002, which is the most complete and accurate national data set available, shows that there are 32 654 fire events (97.7%), with areas ranging from 0.00012 to 1 km^2 [43], [46]. These small fire events account for only 9% of the total burned area in CONUS. If all of these fire events are detected from satellites and if each fire count (removing multiple counts) in a pixel is assumed to be 1 km^2 [50]–[52], 0.84 km^2 [18], and 0.75 km^2 [53], the burned areas in these small fire events could be greatly overestimated. If the fire detection rate is 40% of small fire events (< 1 km^2), as shown in Fig. 10, the burned area for such small fire events would still be overestimated by a factor of ten if the rate of burned area in a fire count is inappropriately used. This uncertainty could result in a large error in total burned areas at a regional scale, which is much higher than the error without consideration of any small fire events. Thus, for the purpose of calculating burned area and biomass burning emissions, we suggest that active fires only observed by multiple satellites once or twice a day should be excluded in order to reduce the overall errors.

ACKNOWLEDGMENT

The authors would like to thank M. Ruminski for providing the HMS data, G. Pouliot for the NFI data, and M. Ruminski, W. Schroeder, and I. Csiszar for the internal reviews. The views, opinions, and findings contained in this paper are those of the authors and should not be interpreted as an official NOAA or U.S. Government position, policy, or decision.

REFERENCES

[1] A. Sapkota, J. M. Symons, J. Kleissl, L. Wang, M. B. Parlange, J. Ondov, P. N. Breysse, G. B. Diette, P. A. Eggleston, and T. J. Buckley, "Impact of the 2002 Canadian forest fires on particulate matter air quality in Baltimore City," *Environ. Sci. Technol.*, vol. 39, no. 1, pp. 24–32, Jan. 2005.

[2] M. A. Cochrane and M. D. Schulze, "Fire as a recurrent event in tropical forests of the eastern Amazon: Effects on forest structure, biomass, and species composition," *Biotropica*, vol. 31, no. 1, pp. 2–16, Mar. 1999.

[3] A. T. Vafeidis and N. A. Drake, "A two-step method for estimating the extent of burned areas with the use of coarse-resolution data," *Int. J. Remote Sens.*, vol. 26, no. 11, pp. 2441–2459, 2005.

[4] T. J. Hawbaker, V. C. Radeloff, A. D. Syphard, Z. Zhu, and S. I. Stewart, "Detection rates of the MODIS active fire product in the United States," *Remote Sens. Environ.*, vol. 112, no. 5, pp. 2656–2664, May 2008.

[5] C. H. Key, "Ecological and sampling constraints on defining landscape fire severity," *Fire Ecol.*, vol. 2, no. 2, pp. 34–59, 2006.

[6] D. P. Roy, Y. Jin, P. E. Lewis, and C. O. Justice, "Prototyping a global algorithm for systematic fire affected area mapping using MODIS time series data," *Remote Sens. Environ.*, vol. 97, no. 2, pp. 137–162, Jul. 2005.

[7] A. T. Vafeidis, N. A. Drake, and J. Wainwright, "A proposed method for modelling the hydrologic response of catchments to burning with the use of remote sensing and GIS," *Catena*, vol. 70, no. 3, pp. 396–409, Aug. 2007, doi: 10.1016/j.catena.2006.11.008.

[8] R. Pu, Z. Li, P. Gong, I. Csiszar, R. Fraser, W. Hao, S. Kondragunta, and F. Weng, "Development and analysis of a 12-year daily 1-km forest fire dataset across North America from NOAA/AVHRR data," *Remote Sens. Environ.*, vol. 108, no. 2, pp. 198–208, 2007.

[9] E. Chuvieco, P. B. Englefield, A. P. Trishchenko, and C. Yi Luo, "Generation of long time series of burn area maps of the boreal forest from NOAA-AVHRR composite data," *Remote Sens. Environ.*, vol. 112, no. 5, pp. 2381–2396, May 2008, doi: 10.1016/j.rse.2007.11.007.

[10] Y. H. Zhang, M. J. Wooster, O. Tutubalina, and G. L. W. Perry, "Monthly burned area and forest fire carbon emission estimates for the Russian Federation from SPOT VGT," *Remote Sens. Environ.*, vol. 87, no. 1, pp. 1–15, Sep. 2003.

[11] K. Tansey, J.-M. Grégoire, P. Defourny, R. Leigh, J.-F. Pekel, E. van Bogaert, and E. Bartholomé, "A new, global, multi-annual (2000–2007) burnt area product at 1 km resolution," *Geophys. Res. Lett.*, vol. 35, p. L01 401, Jan. 2008, doi: 10.1029/2007GL031567.

[12] D. P. Roy, P. E. Lewis, and C. O. Justice, "Burned area mapping using multi-temporal moderate spatial resolution data—A bi-directional reflectance model-based expectation approach," *Remote Sens. Environ.*, vol. 83, no. 1/2, pp. 263–286, Nov. 2002.

[13] D. P. Roy, L. Boschetti, C. O. Justice, and J. Ju, "The collection 5 MODIS burned area product—Global evaluation by comparison with the MODIS active fire product," *Remote Sens. Environ.*, vol. 112, no. 9, pp. 3690–3707, Sep. 2008.

[14] C. H. Key and N. C. Benson, "Measuring and remote sensing of burn severity," in *Proc. Joint Fire Sci. Conf. Workshop*, L. F. Neuenschwander and K. C. Ryan, Eds., Boise, ID, Jun. 15–17, 1999, vol. 2, University of Idaho and International Association of Wildland Fire. 284 pp.

[15] J. Epting, D. Verbyla, and B. Sorbel, "Evaluation of remotely sensed indices for assessing burn severity in interior Alaska using Landsat TM and ETM+," *Remote Sens. Environ.*, vol. 96, no. 3/4, pp. 328–339, Jun. 2005.

[16] R. J. Scholes, J. D. Kendall, and C. O. Justice, "The quantity of biomass burned in Southern Africa," *J. Geophys. Res. Atmos.*, vol. 101, no. D19, pp. 23 667–23 676, 1996.

[17] E. S. Kasischke, J. H. Hewson, B. Stocks, G. R. van der Werf, and J. T. Randerson, "The use of ATSR active fire counts for estimating relative patterns of biomass burning—A study from the boreal forest region," *Geograph. Res. Lett.*, vol. 30, no. 18, p. 1969, 2003, doi: 10.1029/2003GL017859.

[18] L. Giglio, G. R. van der Werf, J. T. Randerson, G. J. Collatz, and P. Kasibhatla, "Global estimation of burned area using MODIS active fire observations," *Atmos. Chem. Phys.*, vol. 6, no. 4, pp. 957–974, 2006.

[19] G. R. van der Werf, J. T. Randerson, L. Giglio, G. J. Collatz, P. S. Kasibhatla, and A. F. Arellano, Jr., "Interannual variability in global biomass burning emissions from 1997 to 2004," *Atmos. Chem. Phys.*, vol. 6, no. 11, pp. 3423–3441, 2006.

[20] A. I. Sukhinin, N. H. F. French, E. S. Kasischke, J. H. Hewson, A. J. Soja, I. A. Csiszar, E. J. Hyer, T. Loboda, S. G. Conard, V. I. Romasko, E. A. Pavlichenko, S. I. Miskiv, and O. A. Slinkina, "Satellite-based mapping of fires in Russia: New products for fire management and carbon cycle studies," *Remote Sens. Environ.*, vol. 93, no. 4, pp. 546–564, Dec. 2004.

[21] X. Zhang and S. Kondragunta, "Temporal and spatial variability in biomass burned areas across the USA derived from the GOES fire product," *Remote Sens. Environ.*, vol. 112, no. 6, pp. 2886–2897, Jun. 2008, doi: 10.1016/j.rse.2008.02.006.

[22] W. Schroeder, E. Prins, L. Giglio, I. Csiszar, C. Schmidt, J. Morisette, C. Justice, and D. Morton, "Validation of GOES and MODIS active fire detection products using ASTER and ETM+ data," *Remote Sens. Environ.*, vol. 112, no. 6, pp. 2711–2726, May 2008.

[23] J. Morisette, L. Giglio, I. Csiszar, and C. Justice, "Validation of the MODIS active fire product over Southern Africa with ASTER data," *Int. J. Remote Sens.*, vol. 26, no. 19, pp. 4239–4264, 2005.

[24] J. Morisette, L. Giglio, I. Csiszar, A. Setzer, W. Schroeder, D. Morton, and C. Justice, "Validation of MODIS active fire detection products derived from two algorithms," *Earth Interactions*, vol. 9, p. EI 141, 2005, Paper No. 9.

[25] I. Csiszar, J. T. Morisette, and L. Giglio, "Validation of active fire detection from moderate-resolution satellite sensors: The MODIS example in Northern Eurasia," *IEEE Trans. Geosci. Remote Sens.*, vol. 44, no. 7, pp. 1757–1764, Jun. 2006.

[26] J. S. Reid, E. J. Hyer, E. M. Prins, D. L. Westphal, J. Zhang, J. Wang, S. A. Christopher, C. A. Curtis, C. C. Schmidt, D. P. Eleuterio, K. A. Richardson, and J. P. Hoffman, "Global monitoring and forecasting of biomass-burning smoke: Description of and lessons from the Fire Locating and Modeling of Burning Emissions (FLAMBE) program," *IEEE J. Sel. Topics Appl. Earth Observations Remote Sens.*, vol. 2, no. 3, pp. 144–162, Sep. 2009.

[27] A. J. Soja, J. Al-Saadi, L. Giglio, D. Randall, C. Kittaka, G. Pouliot, J. J. Kordzi, S. Raffuse, T. G. Pace, T. E. Pierce, T. Moore, B. Roy, R. B. Pierce, and J. J. Szykman, "Assessing satellite-based fire data for use in the National Emissions Inventory," *J. Appl. Remote Sens.*, vol. 3, no. 1, p. 031 504, May 2009, doi: 10.1117/1.3148859.

[28] L. Boschetti, P. A. Brivio, H. D. Eva, J. Gallego, A. Baraldi, and J. M. Gregoire, "A sampling method for the retrospective validation of global burned area products," *IEEE Trans. Geosci. Remote Sens.*, vol. 44, no. 7, pp. 1765–1773, Jul. 2006.

[29] M. Ruminski, S. Kondragunta, R. Draxler, and J. Zeng, "Recent changes to the Hazard Mapping System," in *Proc. 15th Emission Inventory Conf. U.S. Environ. Protection Agency*, New Orleans, LA, May 2006.

[30] W. Schroeder, M. Ruminski, I. Csiszar, L. Giglio, E. Prins, C. Schmidt, and J. Morisette, "Validation analyses of an operational fire monitoring product: The Hazard Mapping System," *International Journal of Remote Sensing*, vol. 29, no. 20, pp. 6059–6066, Oct. 2008.

[31] J. Dozier, "A method for satellite identification of surface temperature fields of sub-pixel resolution," *Remote Sens. Environ.*, vol. 11, pp. 221–229, 1981.

[32] E. M. Prins and W. P. Menzel, "Geostationary satellite detection of biomass burning in South America," *Int. J. Remote Sens.*, vol. 13, no. 15, pp. 2783–2799, 1992.

[33] E. M. Prins and W. P. Menzel, "Trends in South American biomass burning detected with the GOES visible infrared spin scan radiometer atmospheric sounder from 1983 to 1991," *J. Geophys. Res.*, vol. 99, no. D8, pp. 16 719–16 735, 1994.

[34] Z. Li, S. Nadon, and J. Cihlar, "Satellite-based detection of Canadian boreal forest fires: Development and application of the algorithm," *Int. J. Remote Sensing*, vol. 21, no. 16, pp. 3057–3069, 2000.

[35] L. Giglio, J. Descloitres, C. O. Justice, and Y. J. Kaufman, "An enhanced contextual fire detection algorithm for MODIS," *Remote Sens. Environ.*, vol. 87, pp. 273–282, 2003.

[36] T. Loboda, K. J. O'Neal, and I. Csiszar, "Regionally adaptable dNBR-based algorithm for burned area mapping from MODIS data," *Remote Sens. Environ.*, vol. 109, no. 4, pp. 429–442, Aug. 2007.

[37] J. Eidenshink, B. Schwind, K. Brewer, Z. Zhu, B. Quayle, and S. Howard, "A project for Monitoring Trends in Burn Severity," *Fire Ecol.*, vol. 3, no. 1, pp. 3–21, 2007.

[38] National Wildfire Coordinating Group, Fire & Aviation Management Homepage, 2007. [Online]. Available: http://famweb.nwcg.gov

[39] E. M. Prins, J. M. Feltz, W. P. Menzel, and D. E. Ward, "An overview of GOES-8 diurnal fire and smoke results for SCAR-B and 1995 fire season in South America," *J. Geophys. Res.*, vol. 103, no. D24, pp. 31 821–31 835, 1998.

[40] W. P. Menzel and E. M. Prins, "Monitoring biomass burning with the new generation of geostationary satellites," in *Biomass Burning and Global Change Remote Sensing, Modeling and Inventory Development, and Biomass Burning in Africa*, vol. 1, J. S. Levine, Ed. Cambridge, MA: MIT Press, 1996, pp. 56–64.

[41] C. O. Justice, L. Giglio, S. Korontzi, J. Owens, J. Morisette, D. P. Roy *et al.*, "The MODIS fire products," *Remote Sens. Environ.*, vol. 83, no. 1/2, pp. 244–262, 2002.

[42] J. F. Weaver, D. Lindsey, D. Bikos, C. C. Schmidt, and E. Prins, "Fire detection using GOES rapid scan imagery," *Weather Forecast.*, vol. 19, no. 3, pp. 496–510, Jun. 2004.

[43] X. Zhang and S. Kondragunta, "Vegetation burned areas derived from multiple satellite-based active fires," in *Proc. SPIE—Remote Sensing Fire, Science Application*, W. M. Hao, Ed., 2008, vol. 7089, pp. 708 90D.1–708 90D.12.

[44] M. A. Friedl, D. K. McIver, J. C. F. Hodges, X. Y. Zhang, D. Muchoney, A. H. Strahler, C. E. Woodcock, S. Gopal, A. Schneider, A. Cooper, A. Baccini, F. Gao, and C. Schaaf, "Global land cover mapping from MODIS: algorithms and early results," *Remote Sens. Environ.*, vol. 83, no. 1/2, pp. 287–302, Nov. 2002.

[45] X. Zhang, S. Kondragunta, C. Schmidt, and F. Kogan, "Near real time monitoring of biomass burning particulate emissions (PM2.5) across contiguous United States using multiple satellite instruments," *Atmos. Environ.*, vol. 42, no. 29, pp. 6959–6972, Sep. 2008.

[46] WRAP, Inter-RPO National 2002 Wildfire Emissions Inventory-Final Work Plan, Air Sciences & EC/R Project No. 178-72005.

[47] W. E. Heilman, B. E. Potter, and J. I. Zerbe, "Regional climate change in the southern United States: The implications for wildfire occurrence," in *The Productivity and Sustainability of Southern Forest Ecosystems in a Changing Environment*, R. A. Mickler and S. Fox, Eds. New York: Springer-Verlag, 1998, pp. 683–699.

[48] S. Korontzi, J. McCarty, T. Loboda, S. Kumar, and C. Justice, "Global distribution of agricultural fires in croplands from 3 years of MODerate resolution Imaging Spectroradiometer (MODIS) data," *Global Biogeochem. Cycles*, vol. 20, no. 2, p. GB2 021, 2006, doi: 10.1029/2005GB002529.

[49] L. Giglio and J. D. Kendall, "Application of the Dozier retrieval to wildfire characterization: A sensitivity analysis," *Remote Sens. Environ.*, vol. 77, no. 1, pp. 34–49, Jul. 2001.

[50] H. Eva and E. F. Lambin, "Remote sensing of biomass burning in tropical regions: Sampling issues and multisensor approach," *Remote Sens. Environ.*, vol. 64, no. 3, pp. 292–315, Jun. 1998.

[51] B. N. Duncan, R. V. Martin, A. C. Staudt, R. Yevich, and J. A. Logan, "Interannual and seasonal variability of biomass burning emissions constrained by satellite observations," *J. Geophys. Res.*, vol. 108, no. D2, p. 4100, 2003, doi: 10.1029/2002JD002378.

[52] C. Wiedinmyer, B. Quayle, C. Geron, A. Belote, D. McKenzie, X. Zhang, S. O'Neill, and K. K. Wynne, "Estimating emissions from fires in North America for air quality modeling," *Atmos. Environ.*, vol. 40, no. 19, pp. 3419–3432, Jun. 2006.

[53] J. Al-Saadi, A. Soja, B. Pierce, C. Kittaka, L. Emmons, S. Kondragunta, X. Zhang, C. Wiedinmyer, T. Schaack, and J. Szykman, "Evaluation of near-real-time biomass burning emissions estimates constrained by satellite active fire detections," *J. Appl. Remote Sens.*, vol. 2, pp. 1–24, 2008, doi: 10.1117/1.2948785.

Xiaoyang Zhang received the B.A. degree in geography from Peking University, Beijing, China, in 1984, the M.S. degree from the Nanjing Institute of Geography and Limnology, Chinese Academy of Sciences (CAS), Nanjing, China, in 1991, and the Ph.D. degree in remote sensing from King's College London, London, U.K., in 1999.

He was a Research Assistant Professor with the Institute of Hydrobiology, CAS; a Research Associate Professor with the Institute of Geodesy and Geophysics, CAS, from 1984 to 1995; and a Research Associate and Research Assistant Professor with the Department of Geography, Boston University, Boston, MA, from 1999 to 2005. As a Senior Research Scientist at Earth Resources Technology Inc., he has been working at the National Oceanic and Atmospheric Administration/National Environmental Satellite, Data, and Information Service through a contract since April 2005. His research interests include satellite remote sensing of vegetation seasonality and biomass burning emissions, climate–vegetation interaction, and land surface modeling.

Shobha Kondragunta received the M.S. degree in chemistry from Florida Atlantic University, Boca Raton, in 1990 and the Ph.D. degree in chemistry from the University of Maryland, College Park, in 1997.

She was a UCAR Postdoctoral Fellow with the Environmental Protection Agency for over a year before joining the National Oceanic and Atmospheric Administration (NOAA)/National Environmental Satellite, Data, and Information Service (NESDIS) in 1999. She is the Principal Investigator of the Air Quality Remote Sensing Program at NOAA/NESDIS/STAR. As the Air Quality Team Leader, her duties involve building multiagency collaborative projects in the area of satellite-based air quality product development and their applications, holding workshops to discuss the status of on-going projects, and briefing management on air quality activities.

Brad Quayle received the B.S. degree in geography (emphasizing in remote sensing and geographic information systems) from Utah State University, Logan, Utah, in 1990.

He was a GIS Specialist with the U.S. Army Corps of Engineers Omaha District for nearly seven years before joining the Geospatial Services and Technology Center, USDA Forest Service, as a GIS Specialist in 1999. Since 2001, he has been a Remote Sensing/GIS Specialist with the Remote Sensing Applications Center, USDA Forest Service, Salt Lake City, UT, with his primary responsibility being the technical management of the center's MODIS direct readout operations and satellite-based active fire detection and mapping program, where he also currently serves as the Rapid Disturbance Assessment and Services Program Leader, overseeing several rapid response disturbance detection/characterization applications and geospatial support programs, including tactical and strategic fire detection and mapping, and postfire burn severity mapping and assessment.